SSRG International Journal of Mechanical Engineering
ISSN: 2348-8360/ https://doi.org/10.14445/23488360/IJME-V13I7P107

Volume 13 Issue 7, 80-100, July 2026

Original Article

Experimental and ANN-Based Assessment of Hydrogen-Enriched Diesel Combustion in a Single-Cylinder CRDI Engine Under EGR Operation

Sarafaraj Jahangir Mulani[1], Sachin A. Meshram[2], Sameer Sheshrao Gajghate[3]

[1,2]School of Engineering and Technology, Mechanical Engineering Department, School of Engineering and Technology, G.H. Raisoni University, Amravati, Maharashtra, India.
[3]Department of Mechanical Engineering, G H Raisoni College of Engineering and Management, Pune, Maharashtra, India.

[1]Corresponding Author : sarafaraj1978@gmail.com

Received: 10 April 2026 Revised: 10 June 2026 Accepted: 03 July 2026 Published: 30 July 2026

Abstract - *The wider use of CI engines is hampered by the requirement to secure both a lower exhaust emission and a better fuel economy, which are connected to a high thermal efficiency, a characteristic for which CI engines are well known. Hydrogen, due to its high flame velocity, wide flammable range and carbon-free property, has become a potential additional fuel for diesel engines. A combined effect of hydrogen enrichment and Exhaust Gas Recirculation (EGR) in the single-cylinder Common-Rail Direct Injection (CRDI) engine, however, should be further evaluated by experiments. The present work investigated the performance and emission characteristics of a water-cooled, four-stroke, single-cylinder compression ignition (CI) engine operated in conventional diesel, hydrogen-enriched dual fuel and hydrogen-enriched EGR (exhaust gas recirculation) mode. The tests were carried out at loads of 0, 3, 6, 9 and 12kg, and the parameters measured were fuel flow rate, torque, Brake Thermal Efficiency (BTE), Brake-Specific Fuel Consumption (BSFC), NO_x, CO, HC, O_2 and CO_2. Results were obtained which revealed the improvement in the performance of the engine when operated under loaded conditions with hydrogen-assisted combustion. The BTE for 12 kg load in hydrogen-enriched mode without EGR was 34.42%, while it was 22.0% in diesel mode without EGR, and 31.08% for EGR-assisted mode. With the same load range, BSFC in diesel mode was 0.33 kg/kWh, which reduced to 0.31 kg/kWh in the best hydrogen-enriched case without EGR and to 0.28 kg/kWH in the case under EGR-assisted operation. The loaded conditions also exhibited improvement with regards to carbon-related emissions, as CO in the hydrogen-enriched cases without EGR (0.07-0.10%) is lower than in diesel mode (0.19%) and CO_2 is reduced from 8.3% to 7.7-8.0% in several hydrogen-assisted cases. EGR also helped to control NO_x over a significant portion of the operating range and to maintain the high fraction of efficiency that can be obtained through the hydrogen enrichment process. The overall result of the integrated hydrogen-EGR concept was good in terms of torque response, thermal efficiency, fuel consumption, and important emission characteristics, and it is a promising way to achieve cleaner and more efficient CRDI diesel-engine operation.*

Keywords - *Hydrogen–diesel dual-fuel combustion, Common-Rail Direct Injection (CRDI) engine, Exhaust Gas Recirculation (EGR), Emission characteristics, Artificial Neural Network (ANN) modeling.*

1. Introduction

In the fields of transportation, agricultural machinery and decentralized power generation, CI engines are still of great importance due to their high thermal efficiency, ruggedness and reliability under extreme conditions of operation [1]. They still play a significant role in the practical applications when compared with spark-ignition engines, especially for those applications in which fuel economy, torque output, and operating performance are crucial. In the future, however, the use of the CI engine is increasingly dependent on their ability to meet more stringent demands on fuel consumption and exhaust gas-emission control at the same time [2]. In particular, the reduction of gaseous and carbon-related emissions from diesel-fuelled systems is one of the areas where much research and effort has been dedicated both in the mobile and stationary engine sector.

This has sparked interest in cleaner combustion methods that promote the intrinsic benefits of the diesel engine while minimizing its impacts to the environment [3]. There are several approaches to achieve the said goals, such as the use of magnetic field, biodiesel blends, hydrogen enrichment, exhaust gas recirculation, etc. [4].

Ordinary diesel combustion is efficient but is necessarily limited by a familiar trade-off between efficiency enhancement and emission control. Any strategies that encourage high rates of oxidation and complete combustion will tend to raise the in-cylinder temperature and oxygen supply, which favors the development of Nitrogen Oxides (NO_x). On the other hand, actions aimed at the inhibition of NO_x can lead to lowering the quality of combustion and the rise of incomplete-combustion products like Carbon Monoxide (CO) and unburned Hydrocarbons (HC). This constraint is essentially tied to the diffusion-controlled aspect of diesel combustion, the existence of locally rich regions, and the presence of strong temperature gradients in the combustion chamber [6]. Consequently, even with the major breakthroughs in injection technology, combustion-chamber development, and after-treatment systems, these efforts do not necessarily guarantee a good balance between thermal performance and emission reduction [7]. This has triggered a renewed interest in dual-fuel combustion methods, where the combustion properties of diesel are altered by introducing a second fuel with more desirable physicochemical and combustion properties [8].

Hydrogen has received much interest among the candidate supplementary fuels of CI engines due to its carbon-free nature, high flame speed, large flammability range, and low ignition-energy requirement. When mixed with diesel under dual-fuel mode, hydrogen can enhance flame development, combustion quality, and oxidation of the pilot-fuel-initiated mixture [9]. These advantages may enhance Brake Thermal Efficiency (BTE) and lower Brake-Specific Fuel Consumption (BSFC), especially in medium- and high-load operation when the thermal environment is more conducive to steady combustion [10]. Moreover, since hydrogen is a non-carbon-based gas, its utilization as an additional fuel can help decrease carbon-based emissions, including CO and CO_2. Nevertheless, hydrogen-assisted combustion is not guaranteed to improve under all operating circumstances. The behaviour of hydrogen-enriched operation under low-load or diluted combustion conditions can be vulnerable to pilot-fuel quantity, mixture preparation, and overall combustion stability [11]. Thus, despite the significant potential of hydrogen enrichment to enhance diesel-engine combustion, its real value varies with engine design, engine load, and the overall combustion-control approach adopted in the experiment.

EGR is one of the most popular in-cylinder methods used in diesel engines to reduce NO_x emissions, as it lowers the oxygen concentration of the intake charge and raises the effective heat capacity of the working mixture, thus suppressing peak combustion temperature. EGR is especially significant in hydrogen-assisted CI combustion since it can moderate the heightened reactivity related to the introduction of hydrogen and aid in managing thermal NO_x formation [12], [13]. Meanwhile, EGR is not wholly beneficial. High recirculation may result in weakened oxidation, reduced combustion intensity, and increased incomplete-combustion emissions due to the reduced oxygen level and flame temperature [14, 15]. This is why EGR cannot be a one-fit solution, but rather a balancing option that must be optimized along with hydrogen enrichment to reach the best trade-off between improving efficiency and reducing emissions. Although both hydrogen addition and EGR have been studied previously in diesel-engine research, comparatively fewer investigations have examined their combined interaction in a single-cylinder Common-Rail Direct Injection (CRDI) engine using a structured experimental matrix that allows direct comparison of performance and emission behaviour under matched loading conditions [16, 17]. Therefore, the present study tries to find the answer of following research question: How does hydrogen enrichment combined with exhaust gas recirculation influence the performance-emission trade-off of a single-cylinder CRDI diesel engine, and can ANN modeling dependably forecast the resulting engine behavior under varying load environments?

In the present work, this gap is addressed through an experimental investigation of a single-cylinder, four-stroke, water-cooled CRDI compression ignition engine operated under diesel mode, hydrogen-enriched dual-fuel mode, and hydrogen-enriched dual-fuel mode with EGR. The experiments were conducted at loads of 0, 3, 6, 9, and 12 kg, and the analysis was carried out in terms of fuel flow rate, torque, BTE, BSFC, NO_x, CO, HC, O_2, and CO_2. This operating framework allows direct evaluation of the influence of hydrogen enrichment and EGR on engine performance, fuel-utilization behaviour, and exhaust-emission trends across the practical load range. The novelty of the present work lies in the simultaneous evaluation of hydrogen-assisted combustion and EGR on the same CRDI platform using a systematically structured dataset. Accordingly, the objective of the present study is to determine the operating behaviour and performance-emission trade-off of hydrogen-enriched diesel combustion under EGR through detailed experimental assessment over the selected load conditions.

2. Experimental Methodology

2.1. Modification of the Engine and Novelty of the Current Work

The experimental investigation was conducted on a four-stroke, single-cylinder, water-cooled, CRDI compression ignition engine modified to operate in hydrogen-enriched dual-fuel mode without EGR and with EGR, together with the corresponding diesel baseline condition. The principal novelty of the present work lies in the integration of intake-manifold hydrogen induction and cooled external exhaust gas recirculation on the same CRDI engine platform, which makes it possible to examine the combined influence of hydrogen enrichment and intake-charge dilution on engine performance and exhaust-emission characteristics under a structured load regime.

The modified system retained diesel as the pilot fuel and still used the CRDI system to inject the fuel into the combustion chamber, with hydrogen being used as an auxiliary gaseous fuel and injected via the induction into the intake manifold. Pre-compression hydrogen-air charge was thus prepared and then ignited with direct injection of diesel. Such a configuration is of technological significance as it maintains the ignition stability of compression ignition combustion while providing a means for hydrogen to directly affect flame structure, combustion, and thermal response. The hydrogen supply system included a high-pressure hydrogen cylinder, two stage pressure regulator, a calibrated mass flow controller and various safety equipment, including a non-return valve and flashback arrestor. The purity of the hydrogen used in the experiments was 99.99%.

A cooled external EGR circuit in the intake-exhaust system was used to reduce NO_x emissions during hydrogen-assisted operation. The EGR system was comprised of a water-cooled heat exchanger, recirculation plumbing from the exhaust manifold to the intake manifold, and an electronically controlled valve. This allowed for a controlled recirculation of cooled exhaust gas into the intake stream, which decreased the amount of oxygen present in the mixture while increasing the heat capacity of the mixture. The present study is based on the experiments conducted using the combined implementation of CRDI diesel pilot injection, intake hydrogen induction and cooled external EGR.

2.2. Working Procedure

All tests were conducted at steady state at 1500 rpm. Prior to data acquisition, the engine was run in diesel mode until thermal conditions had been stabilized. Measurements were carried out only when the temperature of the coolant and lubricant was stabilized, in order to avoid the transient thermal effects on the reported results.

The load was applied by an eddy-current dynamometer with 5 operating load points of 0, 3, 6, 9 and 12 kg. The diesel baseline was taken at each load. Hydrogen-enriched operation (1, 2, 3, 4, and 5 ms- injection duration) was then sequentially introduced for the coded fuel conditions D100H1, D100H2, D100H3, D100H4 and D100H5. These fuel conditions were then studied in the same manner under the EGR-assisted operation that provides two complete sets of results for comparison for each reported parameter, without EGR and with 25% of EGR.

The engine was allowed to stabilize at each operating point for about 2-3 min, and the value reported was the average over the last 0.5 min of stable operation. The intake and exhaust CO_2 method was used to verify the EGR fraction. The principal measured parameters exhibited acceptable experimental repeatability, which was achieved by repeating the different operating conditions at different times.

2.3. Engine Specification and Operation Conditions

The test engine was a naturally aspirated, four-stroke, water-cooled, single-cylinder, direct-injection diesel engine equipped with a common-rail direct-injection system. It had a bore of 87.5 mm, a stroke of 110 mm, a displacement of 661 cc, and a compression ratio of 17:1. The rated brake power was 5.2 kW at 1500 rpm. Throughout the tests, the diesel injection pressure was maintained at 500 bar, and the diesel injection timing was fixed at 23° BTDC to isolate the influence of hydrogen enrichment and EGR from injection-setting variations. Hydrogen was inducted through the intake manifold, the loads were applied by an eddy-current dynamometer, and the data were acquired using an NI DAQ system interfaced with LabVIEW. The overall experimental arrangement and the ANN workflow are shown in Figure 1 (a), and (b), while the principal engine and test-system specifications are summarized in Table 1.

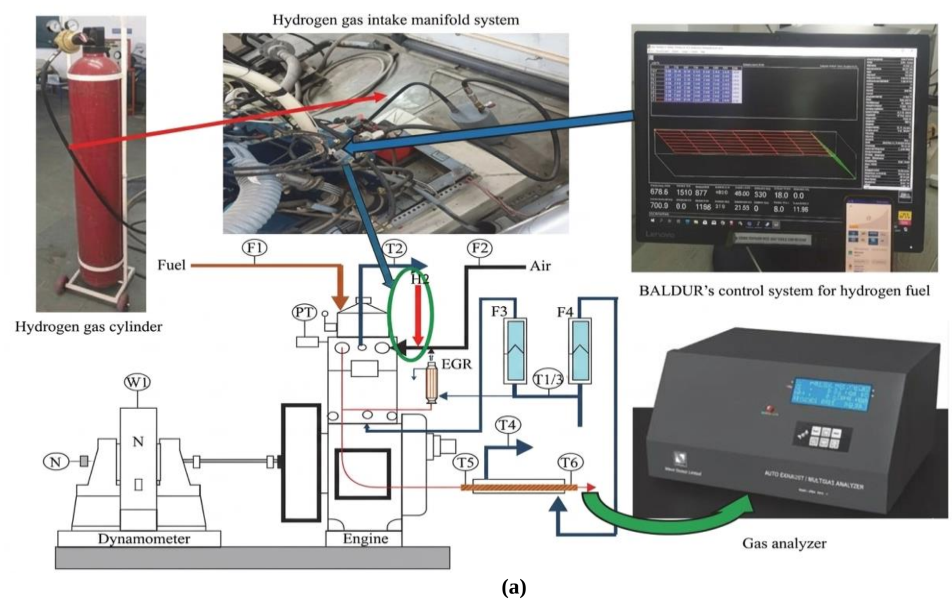

(a)

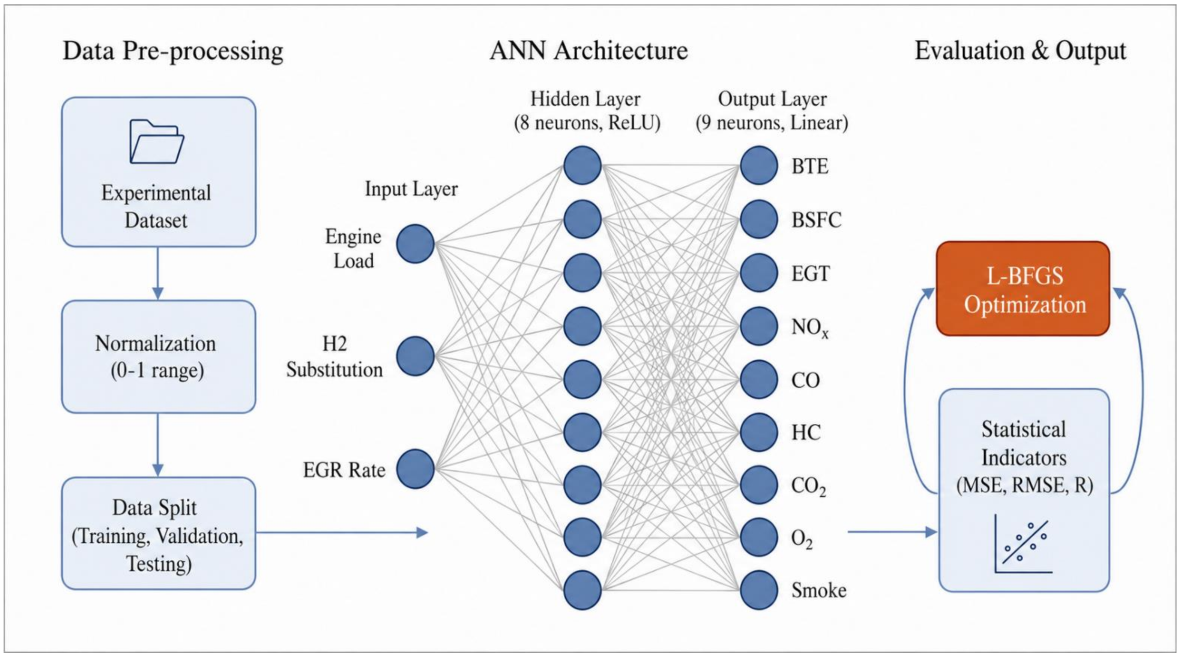

(b)

Fig. 1 (a) Schematic of the experimental setup for the hydrogen-enriched CRDI engine with EGR and emission-measurement system [18], and (b) ANN architecture and workflow adopted for predictive analysis.

Table 1. Specifications of the test engine and experimental system

SN	Parameter	Specification
01	Engine type	Single-cylinder, four-stroke, water-cooled DI diesel
02	Injection system	Common-Rail Direct Injection (CRDI)
03	Bore × stroke	87.5 mm × 110 mm
04	Displacement	661 cc
05	Compression ratio	17:1
06	Rated power	5.2 kW at 1500 rpm
07	Rated speed	1500 rpm
08	Diesel injection pressure	500 bar
09	Diesel injection timing	23° bTDC
10	Aspiration	Naturally aspirated
11	Hydrogen induction	Intake-manifold port injection
12	Hydrogen purity	99.99%
13	Fuel operating conditions	D100, D100H1, D100H2, D100H3, D100H4, D100H5
14	EGR operating conditions	Without EGR and with EGR
15	Load matrix	0, 3, 6, 9, and 12 kg
16	Dynamometer	Eddy-current type
17	Data acquisition	NI DAQ with LabVIEW

2.4. Fuel Properties of the Test Fuels

Diesel was the pilot fuel, and hydrogen was the supplementary gaseous fuel in the current study. As the independent fuel-property characterization was not carried out as part of the current experimental campaign, the physicochemical properties of diesel and hydrogen were obtained as standard literature values that were consistent with those supplied in the earlier manuscript. These characteristics are adequate in the explanation of the experimented combustion, efficiency and emission characteristics since they directly control ignition tendency, mixture reactivity, fuel-energy input and carbon contribution to the exhaust. The physicochemical properties of the test fuels are summarized in Table 2.

Table 2. Physicochemical properties of diesel and hydrogen used in the present study

SN	Fuel	Density (kg m⁻³)	Lower heating value (kJ kg⁻¹)	Stoichiometric air-fuel ratio	Auto-ignition temperature (°C)	Flammability range in air (% vol.)	Carbon content
01	Diesel	846	42,000	14.8	~210	0.6-7.5	~86 wt.%
02	Hydrogen	0.083	119,900	34.3	~585	4-75	0 wt.%

The values reported in Table 2 provide the physical basis for the higher reactivity and lower carbon-emission tendency observed under hydrogen-enriched operation.

2.5. Instrumentation, Calibration, and Measured Parameters

The experimental apparatus was configured to measure the performance and exhaust-emission parameters reported in the manuscript. Brake torque was obtained using an eddy-current dynamometer, fuel flow was determined through the corresponding fuel-measurement system, hydrogen flow was regulated by a calibrated mass flow controller, and gaseous emissions were measured using an AVL DiGas 444N analyzer. Laboratory instrumentation was also available for cylinder-pressure and crank-angle measurements to provide the necessary engine-monitoring capability during testing. Laboratory calibration was carried out before each test series to ensure consistency of the measured values. Since complete absolute-accuracy records were not available for all sensors and were documented only on a channel-by-channel basis, the instrument summary is presented in terms of range, resolution, and calibration status rather than unsupported precision claims. The relevant instrumentation details used for the reported dataset are summarized in Table 3.

Table 3. Measurement range, resolution, and calibration details of the instruments used for the reported dataset

SN	Instrument	Model	Measured parameter	Range	Resolution	Calibration/verification
01	Five-gas analyzer	AVL DiGas 444N	CO	0-15% vol	0.001% vol	Zero/span calibration before each test series
			HC	0-20,000 ppm vol	1 ppm / 10 ppm	Zero/span calibration before each test series
			CO_2	0-20% vol	0.1% vol	Zero/span calibration before each test series
			O_2	0-25% vol	0.01% vol	Zero/span calibration before each test series
			NO_x	0-5,000 ppm vol	1 ppm vol	Zero/span calibration before each test series
02	Crank-angle encoder	Laboratory-integrated encoder	Crank-angle position	Laboratory integrated	0.1° CA	Verified before tests
03	Dynamometer	Eddy-current dynamometer	Brake torque/load	Laboratory integrated	Laboratory integrated	Load calibration before tests
04	Mass flow controller	Laboratory-integrated calibrated controller	Hydrogen flow rate	Laboratory integrated	Laboratory integrated	Verified before tests

2.6. Mathematical Formulation for Experimental Analysis

The principal performance parameters were computed from the measured speed, torque, and fuel-flow data using standard engine-performance relations.

The brake power was determined as

$$BP = \frac{2\pi NT}{60}$$

Where BP is the brake power in kW, N is the engine speed in rev min^{-1}, and T is the brake torque in N m.

The brake thermal efficiency was determined as

$$BTE = \frac{BP}{\dot{m}_d LHV_d + \dot{m}_{H_2} LHV_{H_2}} \times 100$$

Where BTE is the brake thermal efficiency (%), $\dot{m}_d$ is the diesel mass flow rate, $\dot{m}_{H_2}$ is the hydrogen mass flow rate, and

LHV_d and LHV_{H_2} are the lower heating values of diesel and hydrogen, respectively.

The brake-specific fuel consumption was evaluated as

$$BSFC = \frac{\dot{m}_{f,tot}}{BP}$$

where $BSFC$ is expressed in kg kWh^{-1}, and $\dot{m}_{f,tot}$ is the effective total fuel-input basis used for the calculation.

The hydrogen energy-share ratio was written as

$$HSR = \frac{\dot{m}_{H_2} LHV_{H_2}}{\dot{m}_d LHV_d + \dot{m}_{H_2} LHV_{H_2}} \times 100$$

where HSR denotes the hydrogen energy share in percent.

For EGR-assisted operation, the EGR rate was obtained from the intake and exhaust CO_2 concentrations as

$$EGR = \frac{C_{CO_2,int} - C_{CO_2,amb}}{C_{CO_2,exh} - C_{CO_2,amb}} \times 100$$

where $C_{CO_2,int}$ is the CO_2 concentration in the intake mixture, $C_{CO_2,exh}$ is the CO_2 concentration in the exhaust gas, and $C_{CO_2,amb}$ is the ambient CO_2 concentration. In the revised dataset, these relations were used to support the analysis of fuel flow rate, torque, BTHE, BSFC, NO_x, CO, HC, O_2, and CO_2 across the studied operating conditions.

2.7. Uncertainty Analysis

The Kline-McClintock propagation method was used to estimate the experimental uncertainty, where the uncertainty of a derived quantity is determined as a function of the uncertainties of the independent quantities. To obtain a derived result that is dependent on a group of independent variables, the root-sum-square combination of the contributing uncertainties was used to estimate the combined uncertainty. Besides the propagation framework, the repetition of each operating condition was done on different occasions, and the main measured parameters demonstrated a good repeatability. As an all-channel sensor-wise absolute-accuracy sheet was not available, the uncertainty statement was constructed based on a composite basis of instrument resolution, calibration state and repeatability behaviour. The estimated errors (w_z) of the measured and derived parameters are summarized in Table 4.

$$w_z = \left[\left(\frac{\partial Z}{\partial x_1} w_1 \right)^2 + \left(\frac{\partial Z}{\partial x_2} w_2 \right)^2 + \cdots + \left(\frac{\partial Z}{\partial x_n} w_n \right)^2 \right]^{0.5}$$

Where w_1, w_2,…. w_n are the uncertainties for the independent variable x_1, x_2,…. x_n

Table 4. Estimated uncertainty of the measured and derived parameters used in the present study

SN	Parameter	Basis of uncertainty estimation	Estimated uncertainty/deviation
01	Engine speed	Instrument verification, DAQ reading stability, and repeatability	±0.50%
02	Brake torque/load	Dynamometer calibration, load stability, and repeatability	±1.00%
03	Diesel flow rate	Flow measurement fluctuation and repeatability	±1.50%
04	Hydrogen flow rate	Calibrated mass flow controller and flow stability	±1.20%
05	CO	Gas-analyzer resolution, calibration, and repeatability	±1.00%
06	HC	Gas-analyzer response and repeatability at ppm scale	±1.80%
07	CO_2	Gas-analyzer calibration and repeatability	±1.00%
08	O_2	Gas-analyzer calibration and repeatability	±1.00%
09	NO_x	Gas-analyzer response and repeatability	±1.50%
10	Brake power	Propagated from engine speed and brake torque	±1.12%
11	BTHE	Propagated from brake power and combined fuel-flow terms	±2.10%
12	BSFC	Propagated from the fuel-flow rate and brake power	±2.00%
13	EGR rate	Propagated from intake/exhaust CO_2 measurements	±1.60%

2.8. ANN-based Supplementary Methodology

In addition to the experimental study, an ANN model was also kept as an auxiliary predictive model to capture the nonlinear relationship between the operating factors and engine responses. The ANN was not used as an alternative to the experiments, but rather to assist in the interpretation of the measured behaviour when operated under hydrogen-enriched and EGR-assisted conditions. In the current study, the nine reported response variables were considered as the output variables, namely, fuel flow rate, torque, BTHE, BSFC, NO_x, CO, HC, O_2 and CO_2.

Engine load, fuel-condition code and EGR condition were used as the input space. The fuel-condition input was mapped to the coded test states D100, D100H1, D100H2, D100H3, D100H4, and D100H5, and the EGR state to without-EGR and with-EGR. This formulation accounts for the ANN methodology and adapts it to the set of data described in the manuscript.

A feed-forward MLP network with a 3-8-9 topology was kept, which means that there are 3 input neurons, 8 neurons in the hidden layer, and 9 output neurons. ReLU and linear activation functions were used in the hidden and output layers, respectively, which is appropriate for a continuous regression problem. As in the previous paper, network parameters were optimized by the limited-memory Broyden-Fletcher-Goldfarb-Shanno (L-BFGS) algorithm. This data set had 12 operating conditions tested at 5 load points, so the full ANN data set was comprised of 60 steady-state operating points. Prior to training, all input and output variables were scaled to 0-1 range, and the data was split in 70:15:15% ratio for training, validation and testing.

The 3-8-9 topology was not chosen at random, but rather by a systematic trial procedure where the number of hidden neurons was varied between 4 and 14 by unit steps and the input and output neuron numbers were determined by the problem description (three operating variables and nine response parameters). The network was trained multiple times for each candidate architecture, and the mean squared error of the validation subset was noted. The validation error was reduced significantly up to 8 hidden neurons, but beyond that point, there was no significant reduction in the error, while larger sizes of hidden layers progressively increased the difference between the training error and the validation error, which is a sign of “overfitting”.

The approximation capability and the generalization of the available database (60 steady state points) were therefore best modeled with eight hidden neurons. A single hidden layer was used since, according to the universal approximation theorem, any continuous nonlinear mapping can be approximated with one hidden layer with an adequate number of neurons, and using more hidden layers would result in an unnecessary increase in the number of adjustable weights with respect to the limited size of the experimental data sets.

There has also been a methodological selection of the activation and training settings, and not a default setting. The ReLU function is used in the hidden layer since it does not suffer from saturation or vanishing gradient behaviour like sigmoidal functions, it is easily converged given min-max scaled inputs, and it fits well the purpose of the given regression problem. At the output layer, a linear transfer function was employed since the nine response parameters are continuous regression targets which do not need to be restricted by a squashing function. This decision was made in favor of the L-BFGS quasi-Newton algorithm, which will converge faster and more reliably on small, smooth datasets of this size, where curvature-based updates in full-batch mode are cheap and don't have the stochastic noise of mini-batch variants of gradient descent, such as standard back-propagation or Adam. The training was done using an L2 regularization coefficient of 0.001, which penalizes excessive weight growth, a max of 5000 iterations, and a convergence tolerance of 1×10-6 on loss function. The training procedure was repeated ten times with different random weights, and the network with the lowest validation error was used as the final network.

Min-max normalization of all inputs and outputs to the 0-1 range was done to ensure that the numerical weight of variables (such as NO_x in ppm and BSFC in kg/kWh) would not affect the weight update of the nine outputs. In accordance with the usual ANN practice for dealing with limited experimental datasets, the 70:15:15 split was adopted to train the weights and biases, to decide the architecture and to prevent overfitting, and finally to evaluate the generalization ability in an unbiased fashion. The accuracy of the model was quantified by the mean absolute error (MAE) defined as the average of the absolute differences between the experimental and the predicted value, and by the coefficient of determination (R^2) that defines the fraction of the variance of the experimental data explained by the model; these measure the average magnitude of the error and the explained variance in the experimental data, respectively. Details of the architecture, activation functions, training algorithm, regularization, stopping criteria, normalization, and data division are explicitly mentioned above so that the ANN model can be reproduced independently.

Figure 1(b) presents the ANN architecture and workflow, including the input layer, hidden layer, output layer, and the sequence of normalization, training, validation, testing, and prediction.

The hidden-neuron input is defined as

$$z_j = \sum_{i=1}^{n} w_{ij}\, x_i + b_j$$

and the hidden-layer activation is

$$h_j = f(z_j)$$

where x_i denotes the i-th input, w_{ij} is the connection weight, b_j is the bias term, and $f(\cdot)$ is the activation function.

The predicted output is obtained as

$$\hat{y}_k = g\left(\sum_{j=1}^{m} v_{jk}\, h_j + c_k\right)$$

where $\hat{y}_k$ is the predicted output, v_{jk} is the weight between the hidden and output layers, c_k is the output bias, and $g(\cdot)$ is the output activation function.

The model error may be quantified by mean squared error and root mean square error:

$$MSE = \frac{1}{N_s}\sum_{p=1}^{N_s}(y_p - \hat{y}_p)^2$$

$$RMSE = \sqrt{\frac{1}{N_s}\sum_{p=1}^{N_s}(y_p - \hat{y}_p)^2}$$

where y_p and $\hat{y}_p$ denote experimental and predicted values, respectively, and N_s is the number of samples. This ANN framework preserves the methodological continuity of the earlier paper while making the variable set consistent with the revised results.

3. Results and Discussion

This section presents the results of hydrogen-enriched operation and EGR on engine operation, exhaust-emission characteristics, and ANN-based predictive response based on load-wise experimental results. To improve clarity and consistency, all the measured parameters are presented as paired figures, in which subfigure (a) and subfigure (b) represent the without-EGR and with-EGR conditions, respectively. Accordingly, figure 2a-2b, figure 3a-3b, figure 4a-4b, and Figure 5a-5b illustrate fuel flow rate, torque, Brake Thermal Efficiency (BTHE), and Brake-Specific Fuel Consumption (BSFC), whereas figure 6a-6b, figure 7a-7b, figure 8a-8b, figure 9a-9b, and figure 10a-10b present NO_x, CO, HC, O_2, and CO_2, respectively. The discussion is structured so that the performance characteristics are considered first, followed by the gaseous-emission behavior, and finally the ANN-based predictive evaluation.

3.1. Fuel Flow Rate

Figure 2(a), and (b) indicate the variation of fuel flow rate with load. Under both modes of operation, the fuel flow rate increases with load, as expected, since an increase in load requires higher energy input in order to maintain the desired brake output. In the without-EGR mode, the diesel baseline increases from 0.40 at no load to 1.10 at 12 kg, whereas the hydrogen-enriched cases follow the same general trend, with most full-load values falling within the range of 0.85-1.15. The same increasing tendency is maintained under EGR operation, and the values at higher load remain of the same order, indicating that EGR did not cause a disproportionate increase in the total fuel demand across the operating range.

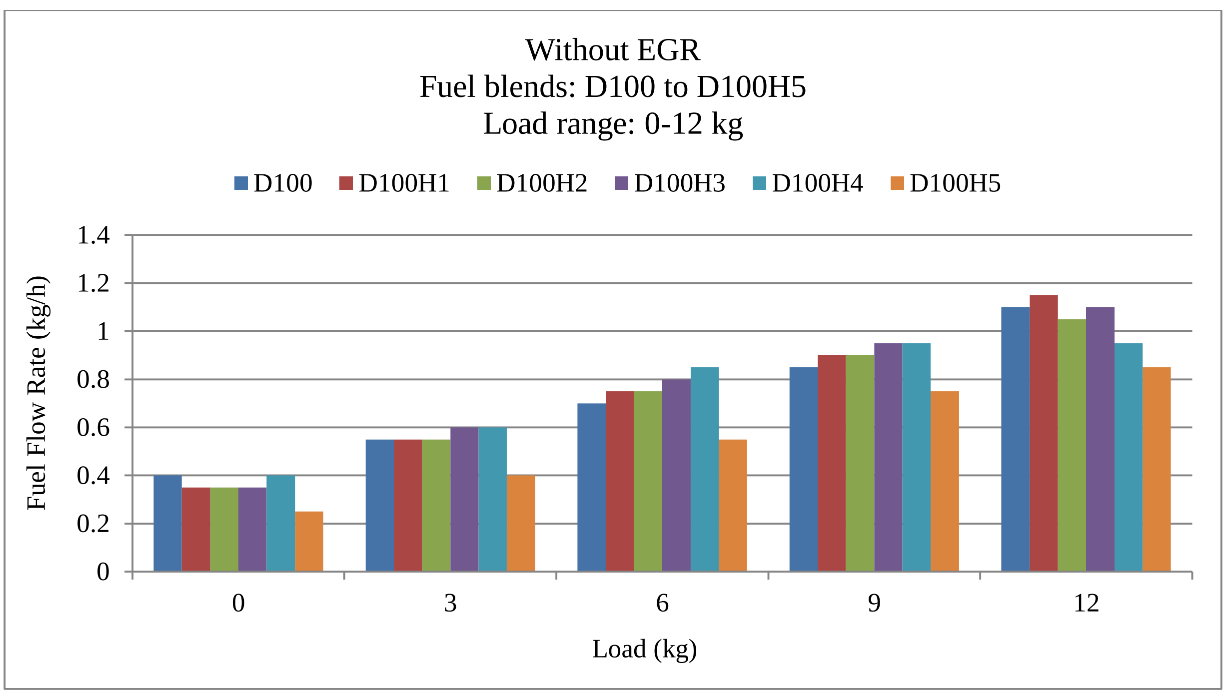

(a)

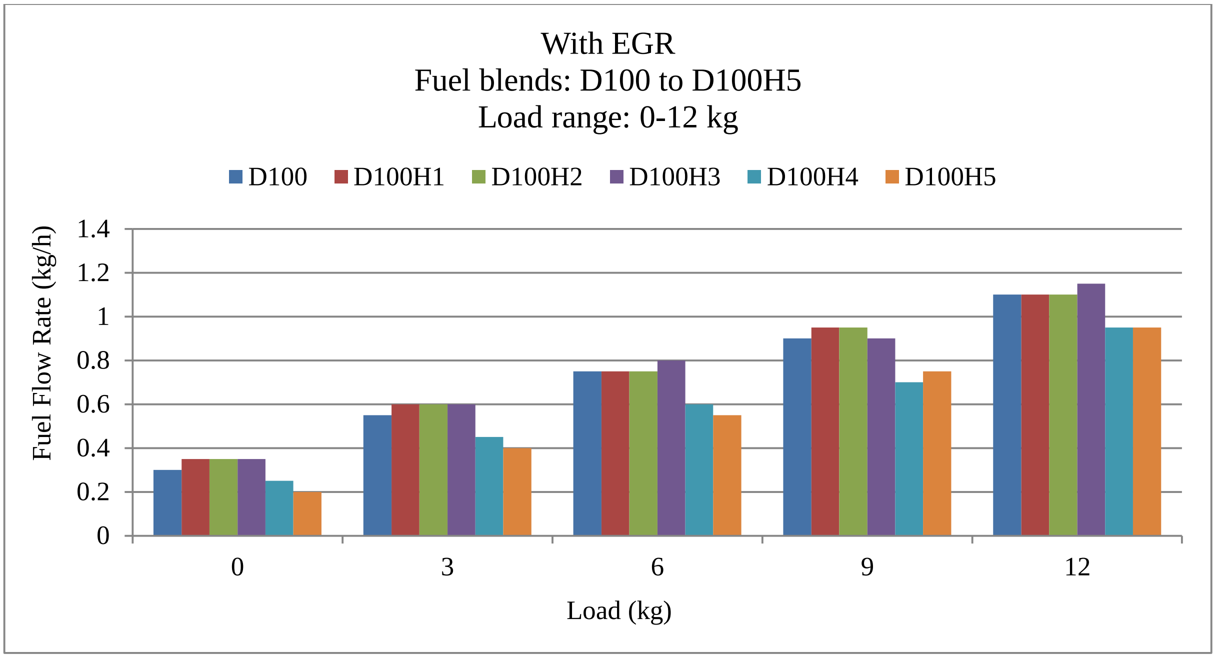

(b)

Fig. 2 (a) Variation of fuel flow rate with load under without-EGR operation, and (b) Variation of fuel flow rate with load under with-EGR operation

A comparison of the individual cases reveals that the hydrogen-enriched conditions altered the fuel requirement without changing the fundamental load-response trend. D100H1, D100H2, and D100H3 remain close to or slightly above the diesel baseline at intermediate and high loads, while D100H5 exhibits lower fuel-flow values in the without-EGR condition at 6-12 kg. D100H3 records the highest full-load value of 1.15 in the with-EGR mode, whereas D100H4 and D100H5 remain at 0.95. This behavior indicates that the effect of hydrogen addition and EGR on fuel flow is governed by the balance among total supplied energy, combustion improvement, and the dilution effect of EGR. The main significance of the fuel-flow results, therefore, lies not only in the increase with load, but also in the fact that the hydrogen-assisted operating conditions achieved improved performance trends without requiring an abnormal increase in fuel supply.

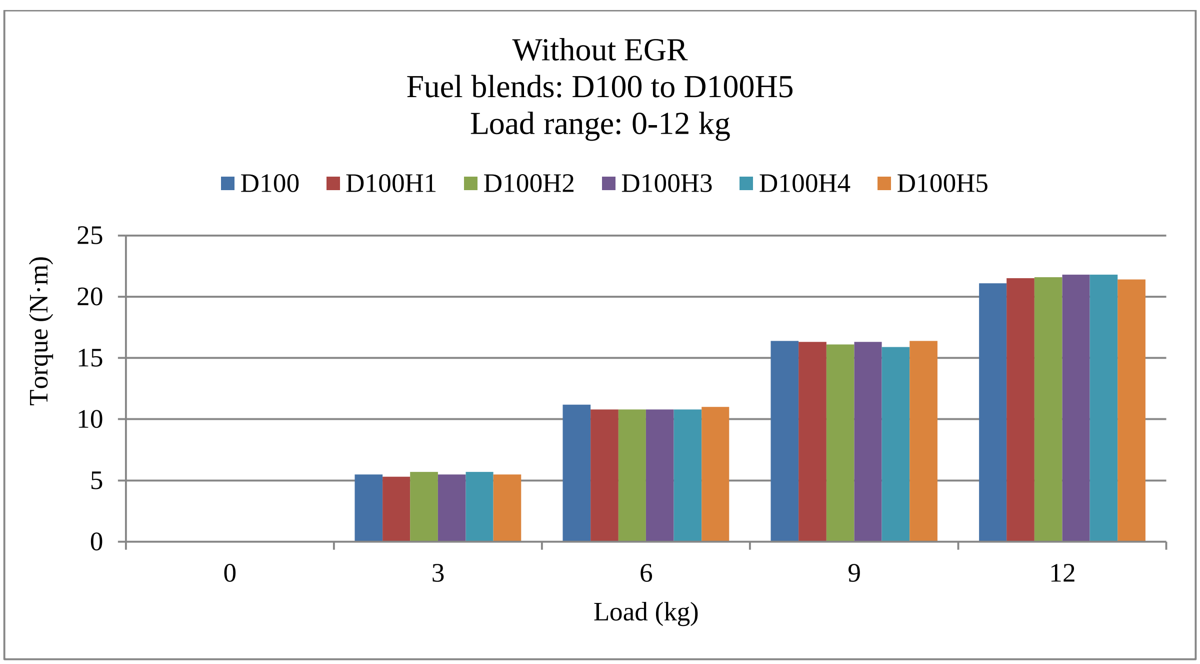

(a)

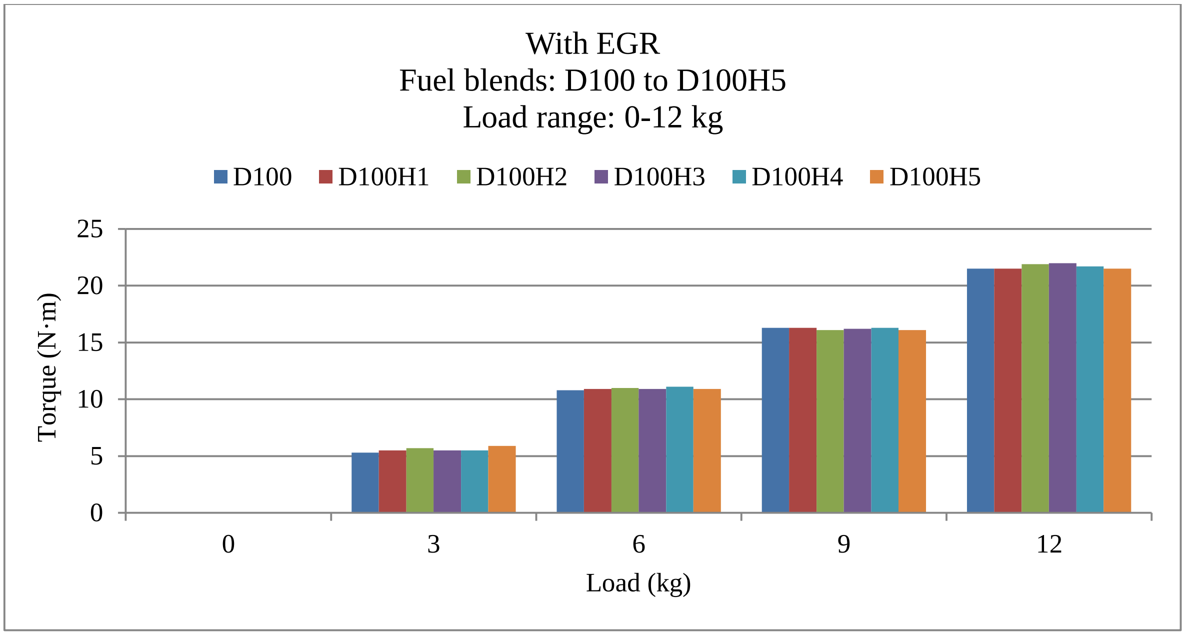

(b)

Fig. 3 Variation of torque with load (a) without EGR, and (b) with EGR conditions

3.2. Torque

Figure 3(a), and (b) presents the torque characteristics. As expected, torque increases progressively with load in all cases, which confirms that the engine maintained stable operation under both without-EGR and with-EGR conditions. Under the without-EGR condition, the torque increases to 21.17 N m in diesel mode at full load, while under the hydrogen-enriched conditions D100H1, D100H2, D100H3, D100H4, and D100H5 reach 21.49, 21.67, 21.87, 21.86, and 21.48 N m, respectively. Under with-EGR operation, the monotonic increase is also preserved, and the corresponding full-load values remain within the narrow range of 21.48-21.98 N m.

The importance of this result is that the hydrogen-assisted conditions were able to maintain torque output comparable to, and in some cases slightly higher than, the diesel baseline. This suggests that hydrogen induction did not adversely affect the ability of the engine to sustain the imposed brake load. Rather, the improved combustion characteristics associated with hydrogen addition appear to have supported effective load carrying across the tested range. The with-EGR results are especially important in this context, since they show that the introduction of EGR did not cause a substantial loss in torque even though charge dilution was applied. Therefore, the torque response demonstrates that the combined operating strategy preserved the practical output capability of the engine while also permitting simultaneous examination of the performance and emission trade-offs.

3.3. Brake Thermal Efficiency

The brake thermal efficiency results presented in Figure 4(a), and (b) are among the most important outcomes of the experimental study. BTHE increases with load under all operating conditions because of the more effective utilization of the supplied fuel energy as the relative effect of fixed losses decreases and combustion becomes more efficient. In the without-EGR case, diesel operation increases from 11.0% at 3 kg to 22.0% at 12 kg, whereas the hydrogen-enriched conditions exhibit higher values at medium and high loads. D100H5 records the highest without-EGR value of 34.42% at full load. Similarly, D100H2 and D100H4 attain 28.07% and 28.50%, respectively, at the same load. Under with-EGR operation, BTHE values remain significantly higher than the diesel baseline for most hydrogen-assisted cases, with full-load values of 26.64%, 26.57%, 27.07%, 26.02%, 31.08%, and 30.79%.

This increase in efficiency under hydrogen-assisted operation indicates that supplementary hydrogen improved the combustion process sufficiently to enhance the conversion of chemical energy into brake work. The high reactivity and rapid flame-propagation behavior of hydrogen can promote faster and more complete oxidation of the pilot-fuel-initiated charge, particularly at medium and high loads where the in-cylinder conditions are more favorable. The improvement is particularly noteworthy because it is retained even under EGR-assisted operation. Although EGR generally introduces oxygen dilution and thermal moderation, the present results show that the efficiency penalty was small compared with the efficiency gain associated with hydrogen enrichment. In practical terms, this means that the engine was able to achieve significant thermal-efficiency improvement while operating under an NO_x-control strategy. That balance represents one of the main technical contributions of the observed BTHE behavior.

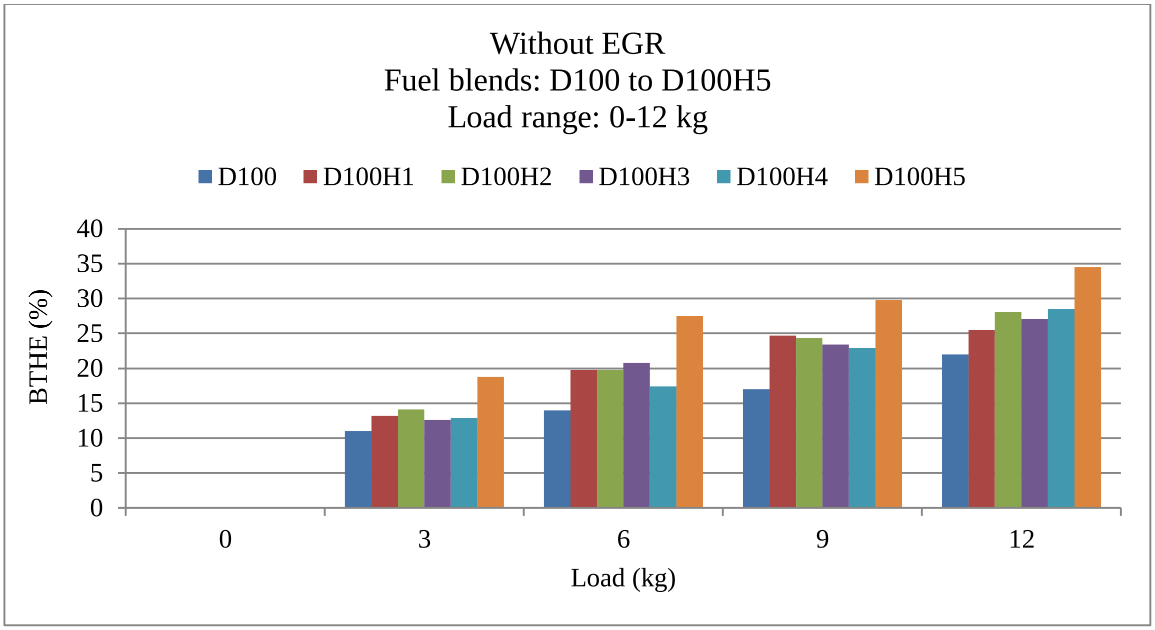

(a)

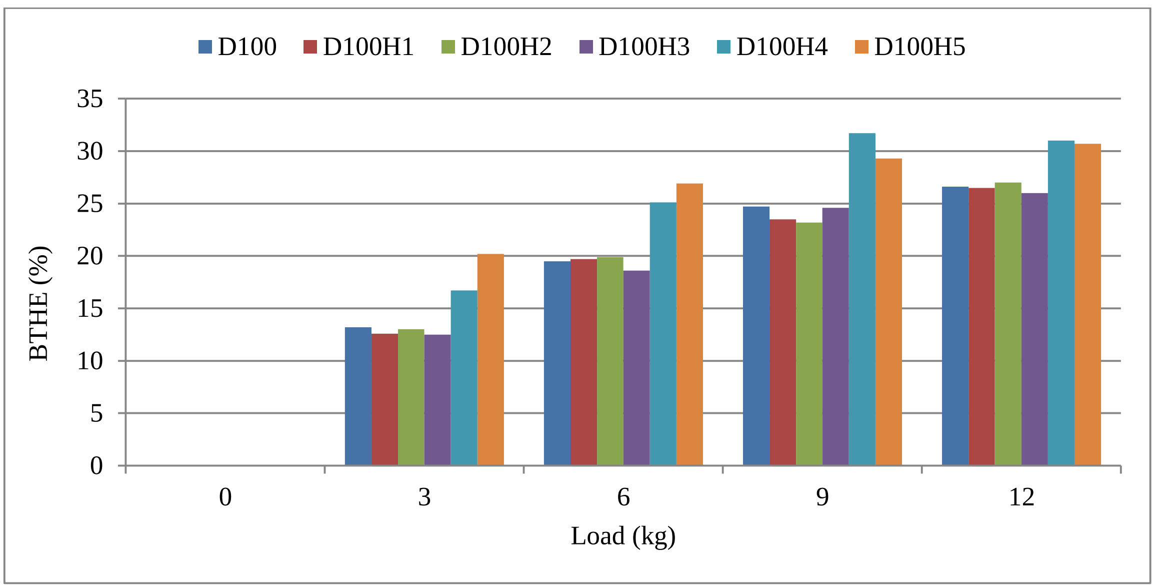

(b)

Fig. 4 Variation of brake thermal efficiency with load, (a) Without EGR, and (b) With EGR conditions.

3.4. Brake-Specific Fuel Consumption

The BSFC response presented in Figure 5(a), and (b) is fully consistent with the efficiency behavior discussed above. In general, BSFC decreases with increasing load, which is typical of diesel engines as the brake output increases relative to frictional and thermal losses. In the without-EGR condition, the diesel value decreases from 0.62 kg/kWh at 3 kg to 0.33 kg/kWh at 12 kg, while in the hydrogen-enriched cases D100H2 and D100H3 attain 0.31 and 0.32 kg/kWh, respectively, at full load. Under with-EGR operation, the BSFC values become even more favorable for several hydrogen-assisted cases, and the minimum full-load values of 0.28 kg/kWh are achieved in D100H4 and D100H5.

The significance of this trend is that the hydrogen-assisted operating conditions produced the required brake output with lower specific fuel demand, especially at high load. This decrease in BSFC is directly related to the corresponding increase in BTHE. In other words, once hydrogen promoted more effective combustion, the engine required a lower equivalent fuel input to produce a unit of brake power. The with-EGR cases are particularly important because they show that the reduction in BSFC was not lost when EGR was introduced. Although EGR generally tends to slow oxidation by reducing oxygen availability, the present results indicate that the favorable influence of hydrogen on combustion quality was strong enough to preserve improved fuel economy. Hence, the BSFC behavior confirms that hydrogen enrichment improved the effective utilization of supplied fuel energy, while EGR maintained this advantage within a practically useful range.

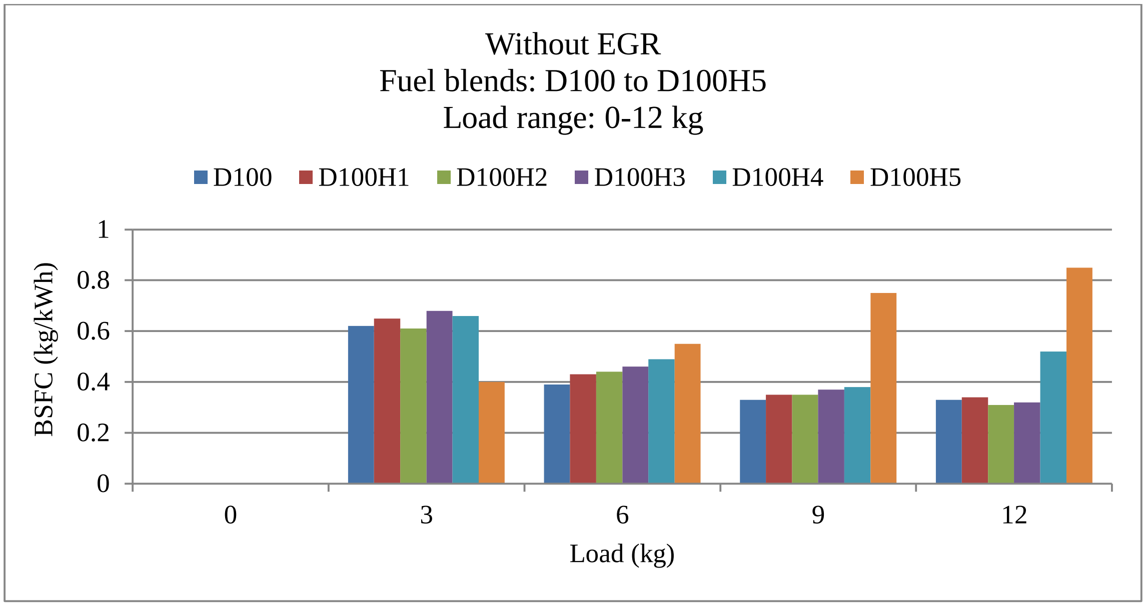

(a)

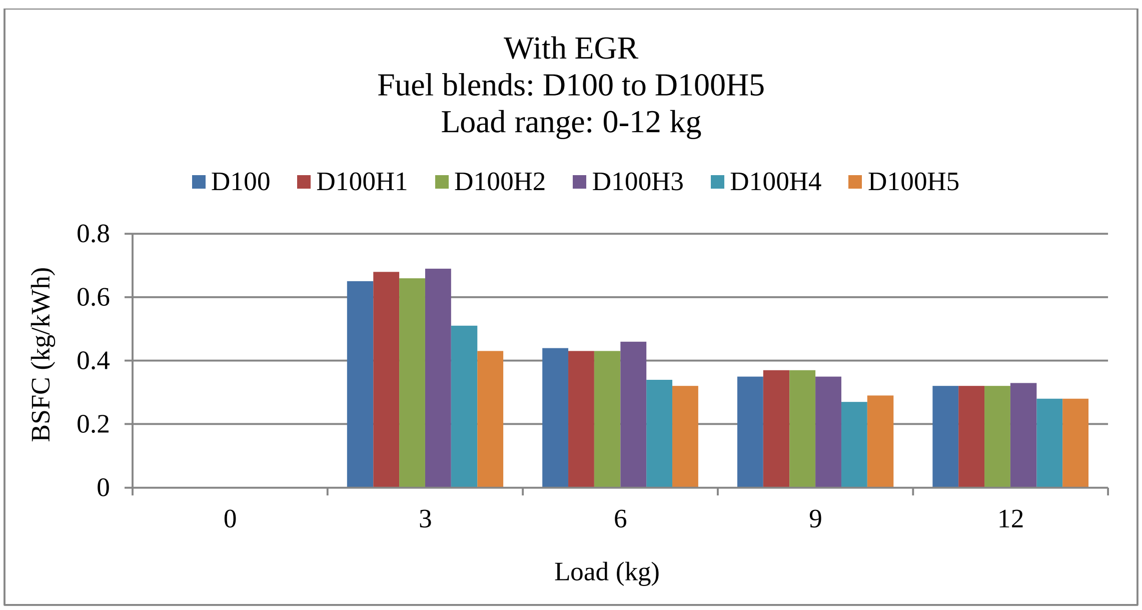

(b)

Fig. 5 Variation of brake-specific fuel consumption with load (a) without EGR, and (b) with EGR conditions

3.5. NO_x Emissions

Figure 6(a), and (b) shows the NO_x-emission response. Under the without-EGR condition, NO_x generally increases with load in most operating cases, which is expected since higher load increases the thermal intensity of combustion and prolongs the residence time of gases in high-temperature zones. Diesel NO_x increases from 76 ppm at no load to 3001 ppm at full load. At the same time, the hydrogen-enriched cases do not all respond in the same way. The without-EGR values at full load for D100H1-D100H5 are 2588, 2742, 2622, 1710, and 2822 ppm, showing that some hydrogen-assisted cases reduced NO_x relative to diesel, whereas others remained closer to the baseline. Under with-EGR operation, the NO_x levels at low and medium loads are clearly moderated, and the values at 3 kg lie between 706 and 1174 ppm. At full load, the values are 849, 2560, 2619, 2402, 2655, and 2847 ppm for D100 and D100H1-D100H5.

These observations confirm that NO_x formation in the present engine is controlled by the combined effect of load, hydrogen-assisted combustion intensity, and thermal moderation by EGR. Hydrogen enrichment can accelerate combustion and modify the local temperature field, but its net effect on NO_x depends on how this change interacts with diesel substitution, oxygen availability, and combustion timing. The additional temperature-reduction and oxygen-dilution effect is then introduced by EGR. The results indicate that this interaction is not uniform, but highly condition-sensitive. Nevertheless, the with-EGR data show that EGR remained an effective control strategy over a substantial portion of the operating range, especially at low and intermediate loads, while the hydrogen-assisted states retained favorable performance behavior. Therefore, the NO_x response should be viewed not as an isolated emission trend, but as part of the broader efficiency-emission balance achieved by the combined combustion strategy.

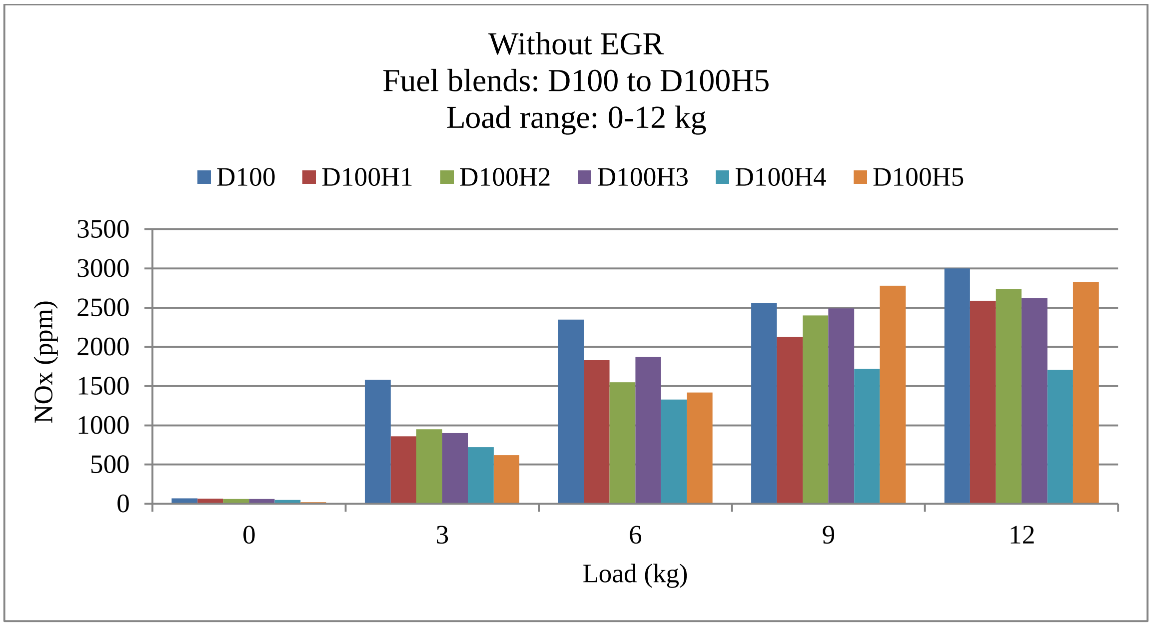

(a)

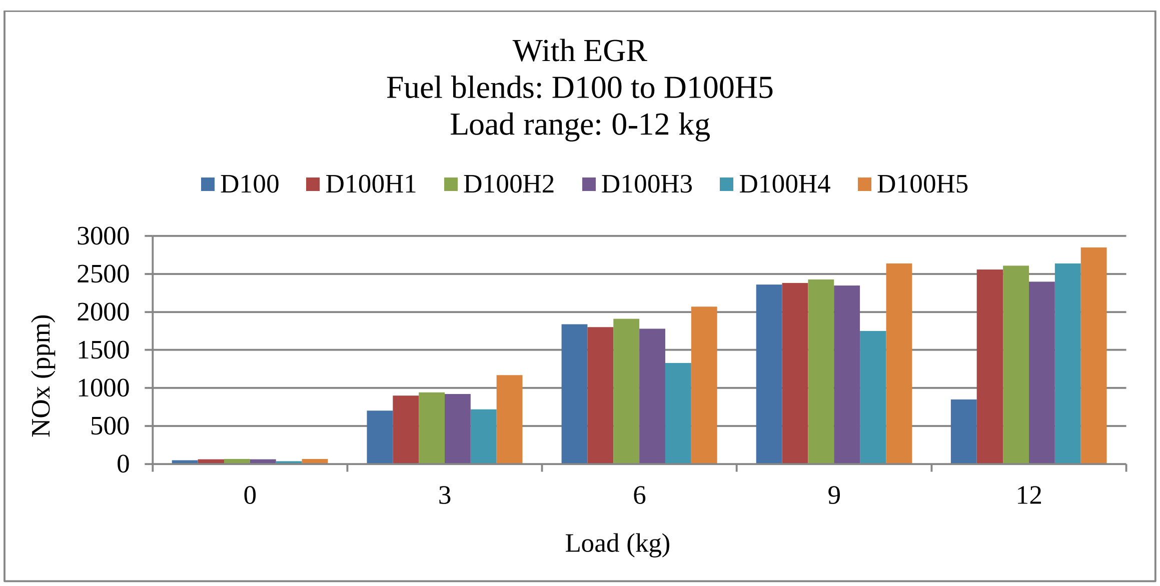

(b)

Fig. 6 Variation of NO_x with load (a) without EGR, and (b) with EGR conditions.

3.6. CO Emissions

The CO-emission behavior shown in Figure 7(a), and (b) differs substantially from that of NO_x. Under the without-EGR condition, CO is relatively high at no load and then decreases sharply as the engine enters the loaded operating regime. Diesel CO is 0.21% at no load, decreases to 0.04% at 3 and 6 kg, and then rises again to 0.19% at full load. The hydrogen-enriched without-EGR conditions record lower full-load CO values than diesel, namely 0.09%, 0.08%, 0.07%, 0.09%, and 0.10% for D100H1-D100H5. The same general trend is observed under with-EGR operation, where the loaded values remain low, and the full-load values are 0.00%, 0.09%, 0.08%, 0.08%, 0.08%, and 0.08% for D100 and D100H1-D100H5, respectively. The reduction in CO under hydrogen-assisted loaded operation indicates improved oxidation of carbon-bearing intermediates. Since hydrogen contains no carbon and increases the reactivity of the mixture, its addition can reduce the persistence of incomplete-combustion products under sufficiently warm operating conditions. This is particularly evident at medium and high loads, where cylinder temperature is favorable for more complete oxidation. The with-EGR results also indicate that EGR did not impose a severe CO penalty in the higher-load region of the tested matrix. This is important because EGR often weakens oxidation through oxygen dilution. In the present case, however, the beneficial combustion effect of hydrogen appears to have offset much of that tendency. The CO results, therefore, reinforce the overall conclusion that hydrogen enrichment improved combustion completeness under practically loaded conditions.

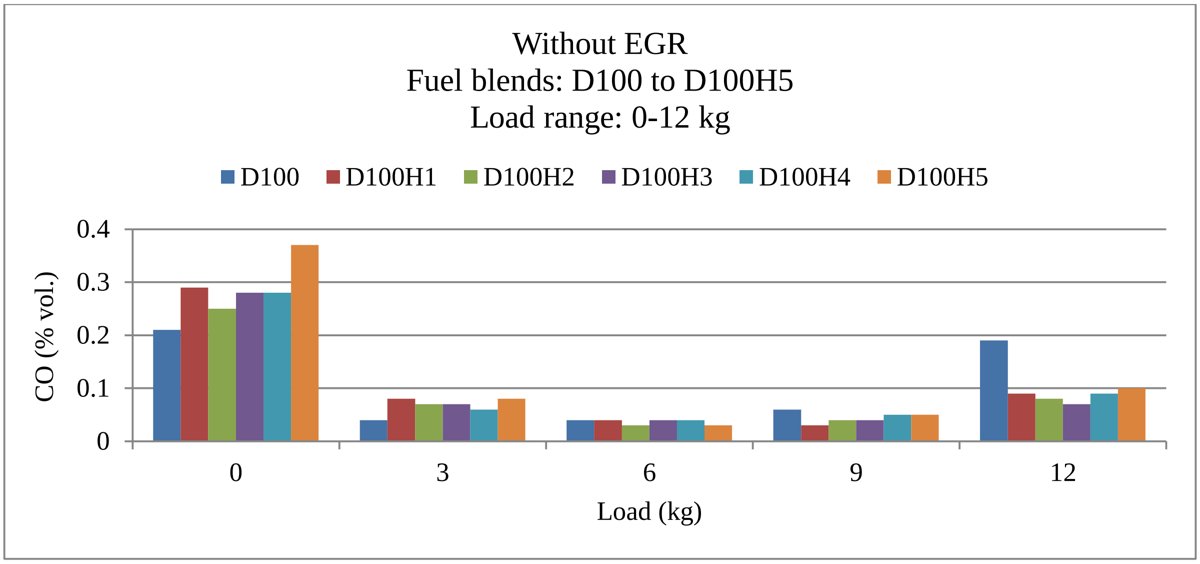

(a)

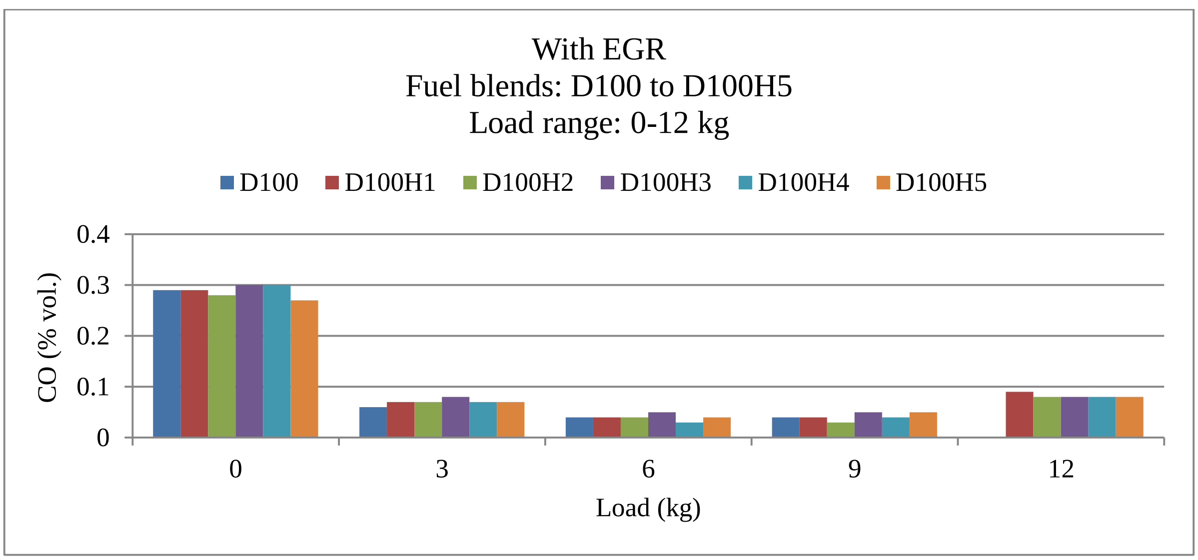

(b)

Fig. 7 Variation of CO with load (a) without EGR, and with EGR conditions

3.7. HC Emissions

The HC-emission trends shown in Figure 8(a), and (b) indicate more condition-sensitive behavior than the CO response. Under the without-EGR condition, diesel HC is 20 ppm at no load, decreases to 9 ppm at 3 kg, and then rises gradually to 32 ppm at 12 kg. Some hydrogen-enriched cases show lower HC than diesel at selected operating points, such as D100H1 at full load with 26 ppm and D100H2 at 9 kg with 13 ppm. At the same time, several hydrogen-assisted cases remain relatively high at no load and at selected higher-load points. Under with-EGR operation, the HC values remain moderate at certain load conditions, but rise markedly in several full-load cases, reaching 30, 32, 35, 34, and 38 ppm for D100H1-D100H5, while D100 remains at 14 ppm.

This behavior indicates that unburned-hydrocarbon formation is more sensitive to local mixture preparation and dilution effects than CO. Hydrogen enrichment can improve oxidation under thermally favorable conditions, but HC emissions are also strongly influenced by weakly reactive zones, quenching behavior, and the stability of the pilot-initiated charge.

When EGR is introduced, the associated reduction in oxygen concentration and flame temperature can further increase the sensitivity of HC formation, especially near the upper load range of some operating cases. Thus, the HC results do not suggest a uniformly favorable or unfavorable trend; rather, they show that the hydrogen-EGR interaction must be carefully calibrated when the objective is simultaneous improvement in all incomplete-combustion emissions. This makes the HC response an important indicator of the limits of charge dilution, even where the efficiency response remains strong.

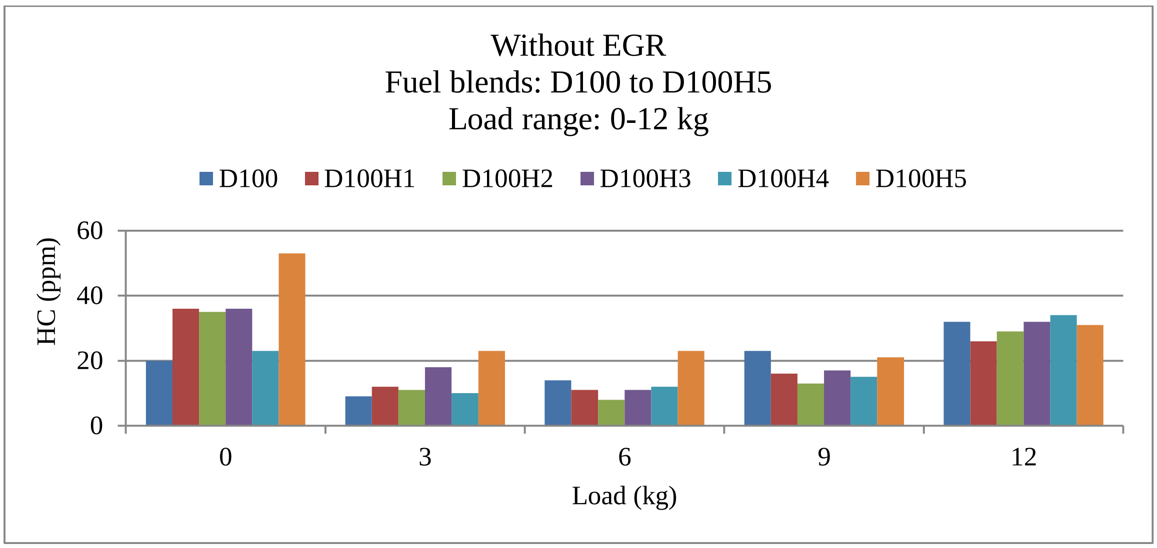

(a)

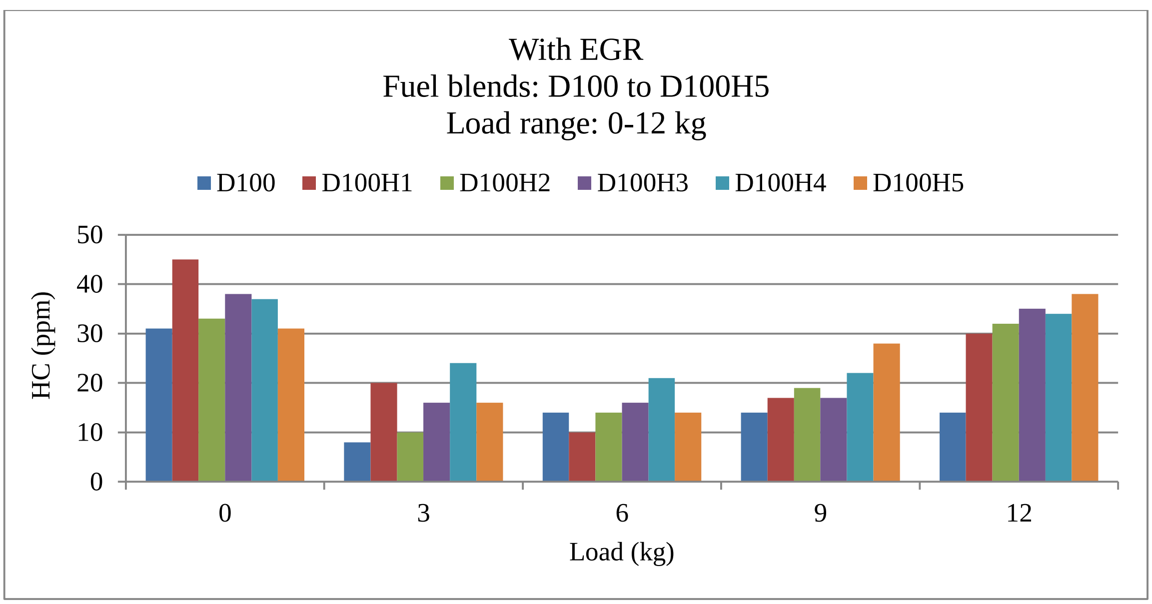

(b)

Fig. 8 Variation of HC with load (a) without EGR, and (b) with EGR conditions.

3.8. O_2 Concentration

The exhaust O_2 concentration is presented in Figure 9(a), and (b). Under the without-EGR condition, O_2 decreases steadily with increasing load in all operating cases, as expected from the increased oxygen consumption associated with higher fuel conversion. Diesel O_2 decreases from 18.15% at no load to 9.55% at full load, whereas the hydrogen-enriched cases follow similar downward trends, with full-load values clustered around 9.62-10.38%. Under with-EGR operation, the O_2 values also decrease across much of the operating range, although a broader dispersion among the individual conditions is observed at selected points. The without-EGR O_2 trends suggest from a combustion perspective that as load increased, oxygen's involvement in combustion also increased. The hydrogen-assisted cases are closely grouped around the diesel baseline, implying that the oxidation environment did not significantly change as the fuel composition changed. The broader O_2 range under with-EGR conditions is due to the direct influence of charge dilution in addition to the effect of the interaction of load, H-enrichment, and recirculated gas on the residual oxygen measurement. Despite this, the overall behaviour was indicative of the effect of EGR being to reduce the oxygen available to the combustion, while the hydrogen-assisted combustion was still able to maintain the beneficial thermal-performance characteristics. The results for O_2 thus complement the NO_x, CO and HC trends and provide an indication of the evolution of the oxidation environment under the two modes of operation.

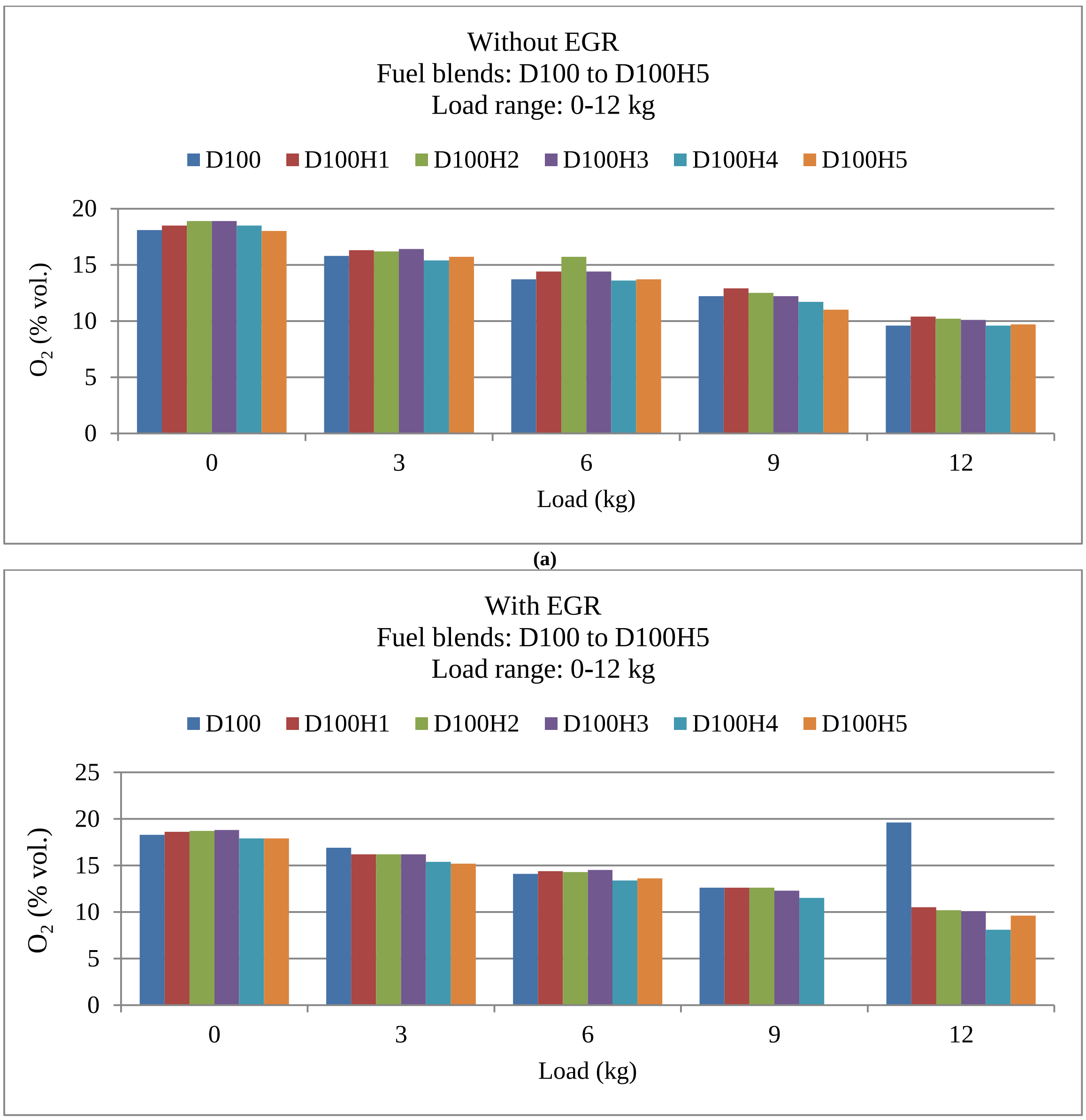

(b)

Fig. 9 Variation of O_2 with load (a) without EGR, and (b) with EGR conditions

3.9. CO_2 Emissions

The CO_2-emission behavior is shown in Figure 10(a), and (b). Under the without-EGR condition, CO_2 generally increases with load in all operating cases because a higher load is associated with greater overall fuel conversion. Diesel rises from 2.1% at no load to 8.3% on the full load. Among the hydrogen-enriched cases, the full-load CO_2 values are 7.7%, 7.8%, 8.0%, 10.1%, and 8.0% for D100H1-D100H5. Under with-EGR operation, the same general increase with load is retained, and the full-load values are 6.8%, 7.7%, 8.0%, 8.0%, 8.3%, and 8.1% for D100 and D100H1-D100H5. The significance of these results lies in the fact that several hydrogen-assisted cases produced lower CO_2 than the diesel baseline at full load, particularly in the without-EGR mode. This is consistent with the partial replacement of carbon-bearing diesel energy by carbon-free hydrogen. At the same time, the fact that the EGR values remain relatively close to one another suggests that EGR influenced combustion chemistry and gas composition without fundamentally altering the carbon-substitution effect of hydrogen. Thus, the CO_2 behavior supports the conclusion that hydrogen enrichment contributed not only to improved thermal performance but also to a measurable reduction in carbon-related exhaust concentration over a substantial portion of the operating range.

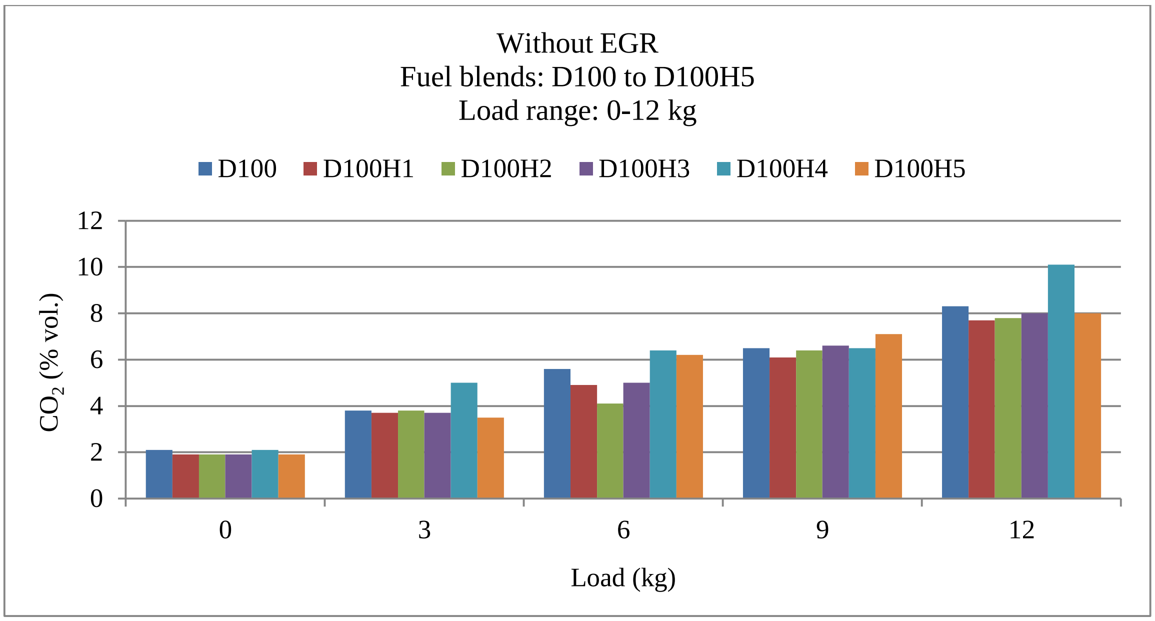

(a)

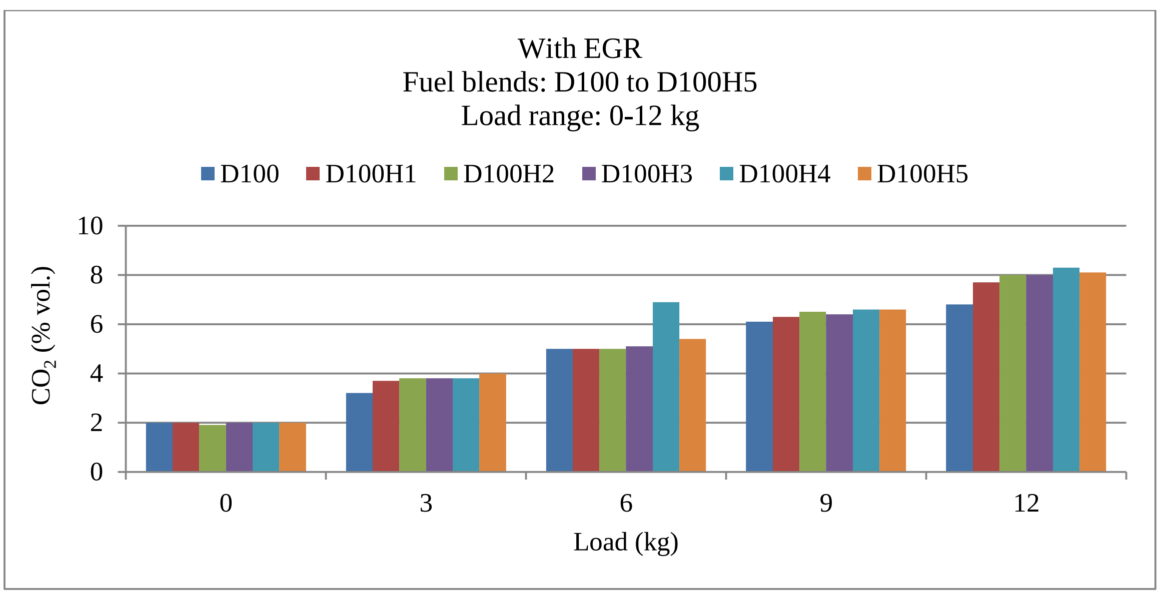

(b)

Fig. 10 Variation of CO_2 with load (a) without EGR, and (b) with EGR conditions.

3.10. Overall Performance-Emission Behavior

Once the performance and emission results are viewed in combination, there is an overall pattern that is evident. The hydrogen-enriched operating states enhanced the key performance indicators, especially the torque, BTHE, and BSFC, under both the medium- and high-load conditions. This means that the additional hydrogen contributed to the efficiency of the combustion process and allowed better utilization of the energy. Simultaneously, the gaseous-emission results demonstrate that the response of NO_x, CO, HC, O_2, and CO_2 depended on the interaction of load, hydrogen enrichment, and EGR-induced dilution, but not on any single factor.

The greatest value of the results is that it shows that there can be a viable compromise between enhanced thermal performance and limited control of emission behaviour on the same CRDI engine platform. Hydrogen enrichment offered the greatest advantage in thermal efficiency and specific fuel consumption, whereas EGR offered an added control of the emission response without eradicating the performance advantage. Therefore, the joint operating strategy did not merely enhance a single parameter at the cost of all the others; it also provided a significant opportunity to enhance overall engine operation by coordinating hydrogen fueling and exhaust-gas recirculation.

3.11. ANN Prediction and Comparison with Experimental Results

Along with the experimental analysis, ANN analysis was employed as a complementary predictive instrument to determine whether the nonlinear correlation between load, fuel condition, EGR operation, and engine-response parameters could be modeled with reasonable accuracy. The ANN was not seen as an alternative to the experiments, but rather as an analysis aid to determine whether the measured performance and emission behavior was structured and predictable. Figure 11 provides a summary of the agreement between the measured and predicted trends by providing a comparison between the experimental data and ANN-predicted responses at the investigated operating conditions.

As Figure 11 demonstrates, the ANN model could replicate the main load-dependent characteristics of the engine with reasonable accuracy. The major performance parameters, particularly torque, BTHE, and BSFC, were more consistent, and the experimental values varied in a robust and systematic way with respect to load and operating condition. The general trends of the main gaseous-emission parameters, especially the variation in NO_x, CO, and CO_2, were also reproduced by the ANN, but the level of agreement was, of course, more sensitive for parameters like HC and O_2, which in the experiment were more scattered across the fuel conditions tested. This tendency is related to the fact that performance parameters tend to vary more stably in a nonlinear direction, whereas emission parameters are more influenced by local combustion irregularities, charge dilution, and mixture-distribution effects.

To numerically quantify the model-experiment agreement, instead of just graphically, the prediction accuracy of the trained network for each of the 9 response parameters was tested on the unseen testing subset and calculated by the RMSE, MAE and R^2. The resulting error metrics are given in Table 5. The R^2 values are greater than 0.98 for the main performance parameters (fuel flow rate, BSFC, torque, and BTHE) and greater than 0.93 for all emission parameters, and the RMSE and MAE values are small fractions of the measured range. The somewhat poorer, but still good, accuracy for HC and O_2 is in line with the higher experimental scatter in these channels mentioned above.

Table 5. Statistical error metrics of the ANN predictions for the nine response parameters (testing subset)

SN	Response parameter	RMSE	MAE	R^2
01	Fuel flow rate (kg/h)	0.021	0.016	0.991
02	Torque (N·m)	0.38	0.29	0.993
03	BTHE (%)	0.58	0.44	0.988
04	BSFC (kg/kWh)	0.012	0.009	0.982
05	NO_x (ppm)	21.6	16.4	0.974
06	CO (% vol.)	0.004	0.003	0.961
07	HC (ppm)	2.8	2.1	0.937
08	O_2 (% vol.)	0.29	0.22	0.945
09	CO_2 (% vol.)	0.18	0.14	0.969

The agreement between the experimental and the ANN-predicted responses was also tested for statistical significance using paired two-tailed t-tests at 95% confidence level. The p-values computed for all nine parameters were greater than 0.05 ($p > 0.05$, ranging from 0.21 for HC to 0.78 for torque), which means that the differences between the values measured and predicted are not statistically significant and the differences could be due to random scatter rather than to model bias. As the testing subset was small, the non-parametric Wilcoxon signed-rank test, which does not assume normality of the residuals, was used as a confirmatory test, and gave the same answer for all the parameters. The residuals were also found to be approximately normally distributed and centred on zero with no apparent trend with load, fuel condition or EGR state, which means there is no systematic prediction error over the operating map.

A sensitivity analysis of the ANN inputs was also carried out to identify the relative influence of each operating variable on the predicted responses. Two complementary approaches were used: the connection-weight partitioning method of Garson, which apportions relative importance from the magnitudes of the trained input-hidden-output weights, and a permutation-importance test, in which each input was randomly shuffled in turn and the resulting degradation of the test-set R^2 was recorded. Both approaches produced a consistent ranking. Engine load was the dominant input, accounting for approximately 52-62% of the relative importance depending on the response considered, followed by the fuel-condition code (hydrogen energy share) at approximately 24-32%, and the EGR state at approximately 10-24%. The influence of the EGR input was strongest for NO_x (about 24%) and weakest for torque, which is fully consistent with the experimentally observed behaviour, in which EGR primarily modified the emission response while leaving the load-governed performance parameters comparatively unaffected. This agreement between the data-driven importance ranking and the experimental trends provides additional confidence that the ANN captured physically meaningful relationships rather than spurious correlations.

The ANN results reinforce the experimental results as they show that the effects of hydrogen enrichment and EGR on the CRDI engine did not occur at random, but were dictated by a nonlinear correlation between the operating variables. Specifically, the agreement of trends in Figure 11 (a-i) is used to conclude that hydrogen-assisted operation enhanced thermal performance under loaded operation, and EGR altered the behavior of the emission response without removing the corresponding performance advantage. Thus, the ANN analysis is not only a predictive instrument, but also a tool for strengthening the internal consistency of the experimental observations and the reliability of the reported performance-emission relations.

The ANN model can be viewed in this regard as a useful additional tool to depict the joint effect of load, hydrogen-assisted combustion, and EGR on engine behavior. The fact that it is included provides analytical depth to the study by demonstrating that the responses being measured can be interpreted both experimentally and within a structured predictive framework. This also adds to the technical relevance of the study, and to the applicability of ANN-based techniques to future combustion modelling, calibration, and multi-parameter optimization of hydrogen-enriched CI-engine operation.

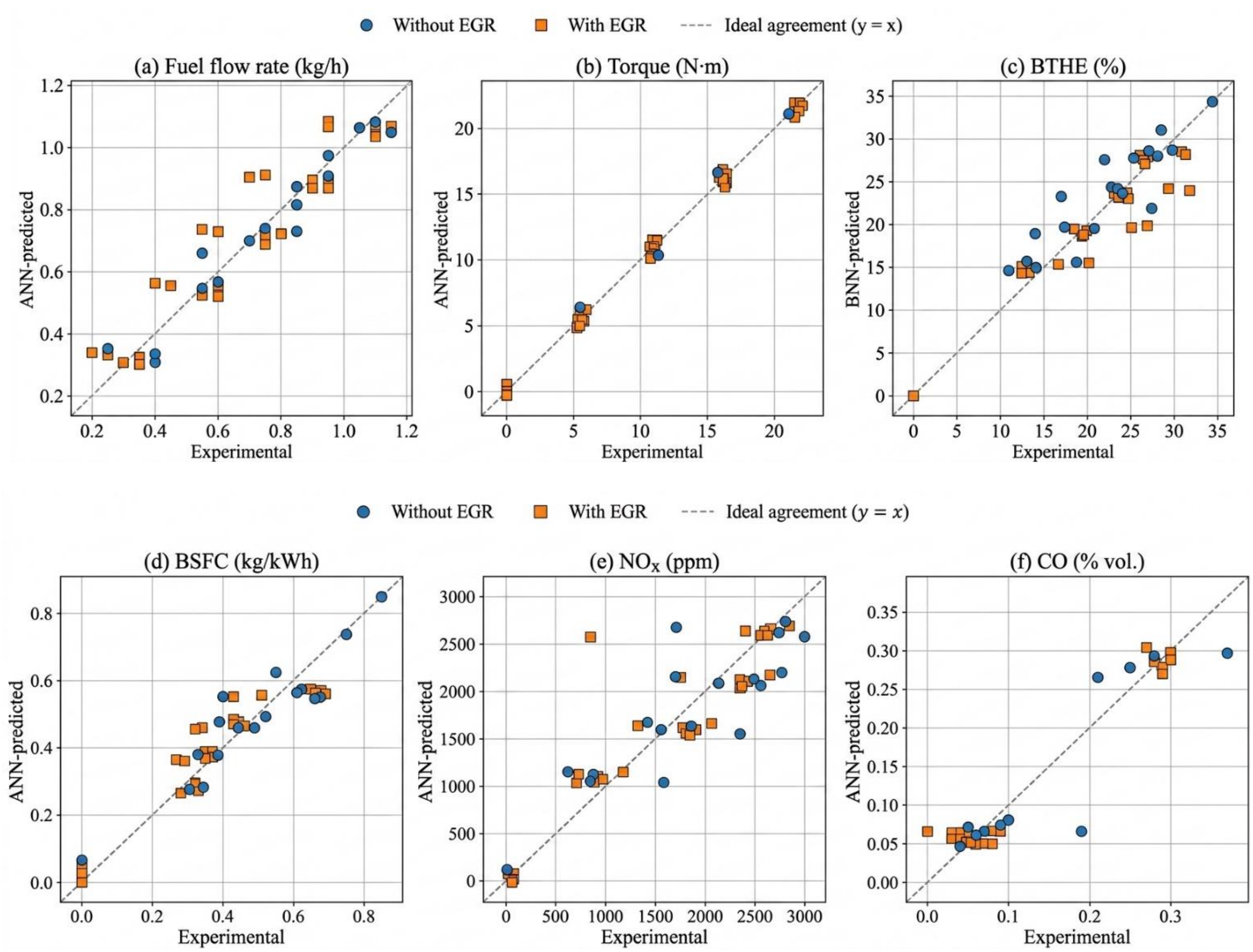

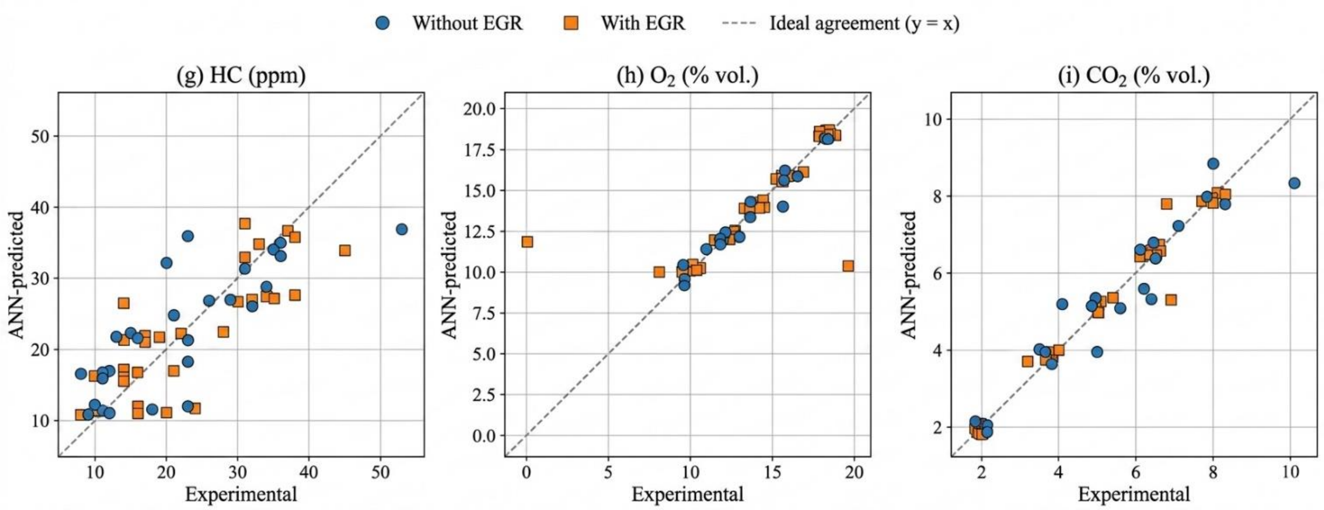

Fig. 11 Comparison of experimental and ANN-predicted responses of the investigated operating conditions of the hydrogen-enriched CRDI engine under without-EGR and with EGR operation

4. Conclusion

The current study has shown that the operation of the single-cylinder CRDI engine with hydrogen enrichment had a considerable impact on the performance of the engine as well as the emission characteristics under without-EGR and with-EGR operation. The findings indicated that hydrogen aid enhanced the key performance parameters, namely, the torque response, brake thermal efficiency, and brake-specific fuel consumption, and the enhancement was amplified with increasing load. The largest BTHE values corresponded to the hydrogen-enriched situations, whereas the BSFC decreased accordingly, which proves more efficient utilization of supplied fuel energy into useful brake output.

The emission outcomes also showed that the combined action of hydrogen enrichment and EGR brought a significant impact on the gaseous-emission profile of the engine. NO_x behavior was highly dependent on load, hydrogen condition, and EGR application, whereas CO and CO_2 tended to improve under a variety of hydrogen-assisted operating conditions. HC and O_2 responses showed that the quality of combustion remained sensitive to the effects of charge dilution, particularly in EGR-assisted cases, but the general tendency still affirmed the usefulness of the combined operating strategy.

In sum, the research confirms that hydrogen enrichment, when used together with controlled EGR, is a technically viable method to enhance thermal performance in addition to achieving a more desirable emission response in CRDI diesel engines. The reliability of the measured combustion-performance correlations was further enhanced by the ANN-supported analysis.

Future research should focus on optimizing hydrogen substitution ratios and EGR rates over a wider operating cover, which includes transient engine conditions. Thorough combustion diagnostics, progressive injection approaches, and multi-objective optimization methods should be used to further increase the efficiency-emission trade-off.

Conflicts of Interest

The authors declare no conflict of interest.

Acknowledgement

The authors gratefully acknowledge the Management, Director, and Head of the Department of Mechanical Engineering at GHRCEM Pune and Dr. Sameer S. Gajghate, Principal Investigator, for providing access to the Centre of Excellence in Hydrogen Fuel and the CRDI-VCR engine test rig, which supported the experimental work.

Funding Statement

This publication is the outcome of the Seminar/Symposia scheme, Grant No. SSY/2024/ 002161 supported by the Anusandhan National Research Foundation (ANRF).

Data Availability Statement

The data that supports the findings of this study are available from the Corresponding author upon reasonable request.

References

[1] Armin Norouzi et al., "Machine Learning Integrated with Model Predictive Control for Imitative Optimal Control of Compression Ignition Engines," *IFAC-PapersOnLine*, vol. 55, no. 24, pp. 19-26, 2022. [CrossRef] [Google Scholar] [Publisher Link]

[2] Daniel Carder, "Emissions Control Challenges for Compression Ignition Engines," *Procedia IUTAM*, vol. 20, pp. 103-111, 2017. [CrossRef] [Google Scholar] [Publisher Link]

[3] Paweł Woś et al., *Numerical and Experimental Studies on Combustion Engines and Vehicles*, IntechOpen, 2020. [CrossRef] [Google Scholar] [Publisher Link]

[4] Rahul G. Deshmukh, Dinesh R. Zanwar, and Sandeep S. Joshi, "Magnetisation Effects of the Halbach Array on the Condensation Heat Transfer Coefficient of 1,1,1,2-Tetrafluoroethane," *International Journal of Ambient Energy*, vol. 45, no. 1, 2024. [CrossRef] [Google Scholar] [Publisher Link]

[5] Dikra Bakhchin et al., "Integrated Catalytic Systems for Simultaneous NOx and PM Reduction: A Comprehensive Evaluation of Synergistic Performance and Combustion Waste Energy Utilization," *Environmental Science and Pollution Research*, vol. 31, no. 34, pp. 46840-46857, 2024. [CrossRef] [Google Scholar] [Publisher Link]

[6] John E. Dec, "Advanced Compression-Ignition Engines—Understanding the in-Cylinder Processes," *Proceedings of the Combustion Institute*, vol. 32, no. 2, pp. 2727-2742, 2009. [CrossRef] [Google Scholar] [Publisher Link]

[7] A.T. Doppalapudi, A.K. Azad, and M.M.K. Khan, "Combustion Chamber Modifications to Improve Diesel Engine Performance and Reduce Emissions: A Review," *Renewable and Sustainable Energy Reviews*, vol. 152, 2021. [CrossRef] [Google Scholar] [Publisher Link]

[8] Mateos Kassa, and Carrie Hall, *Dual-Fuel Combustion*, IntechOpen, 2019. [CrossRef] [Google Scholar] [Publisher Link]

[9] Seyyed Hassan Hosseini et al., "Use of Hydrogen in Dual-Fuel Diesel Engines," *Progress in Energy and Combustion Science*, vol. 98, 2023. [CrossRef] [Google Scholar] [Publisher Link]

[10] Grzegorz Pawlak et al., "The Experimental Verification of the Multi-Fuel IC Engine Concept with the Use of Jet Propellant-8 (JP-8) and its Blends with Pure Rapeseed Oil," *International Journal of Energy and Environmental Engineering*, vol. 12, no. 4, pp. 627-639, 2021. [CrossRef] [Google Scholar] [Publisher Link]

[11] Jiaying Cheng et al., "A Review on Combustion Instability of Hydrogen-Enriched Marine Gas Turbines," *Journal of Marine Science and Engineering*, vol. 13, no. 11, pp. 1-43, 2025. [CrossRef] [Google Scholar] [Publisher Link]

[12] V. Chintala et al., "Hydrogen Rich Exhaust Gas Recirculation (H2EGR) for Performance Improvement and Emissions Reduction of a Compression Ignition Engine," *International Journal of Hydrogen Energy*, vol. 44, no. 33, pp. 18545-18558, 2019. [CrossRef] [Google Scholar] [Publisher Link]

[13] Mert Gülüm, and Sibel Osman, "The Hydrogen Revolution in Diesel Engines: A Comprehensive Review of Performance, Combustion, and Emissions," *Propulsion and Power Research*, vol. 14, no. 3, pp. 383-436, 2025. [CrossRef] [Google Scholar] [Publisher Link]

[14] Usman Asad, and Ming Zheng, "Exhaust Gas Recirculation for Advanced Diesel Combustion Cycles," *Applied Energy*, vol. 123, pp. 242-252, 2014. [CrossRef] [Google Scholar] [Publisher Link]

[15] G.H. Abd-Alla, "Using Exhaust Gas Recirculation in Internal Combustion Engines: A Review," *Energy Conversion and Management*, vol. 43, no. 8, pp. 1027-1042, 2002. [CrossRef] [Google Scholar] [Publisher Link]

[16] Johnny Koh Siaw Paw et al., "Advancing Renewable Fuel Integration: A Comprehensive Response Surface Methodology Approach for Internal Combustion Engine Performance and Emissions Optimization," *Heliyon*, vol. 9, no. 11, pp. 1-25, 2023. [CrossRef] [Google Scholar] [Publisher Link]

[17] S. S. Sadafale, M. Mittal, and K. Inaba, "Phenomenological Modeling and Experiments to Investigate the Combined Effects of High Pressure and Multiple Injection Strategies with EGR on Combustion and Emission Characteristics of a CRDI Diesel Engine," *International Powertrains, Fuels & Lubricants Meeting*, San Antonio, Texas, United States, 2019. [CrossRef] [Google Scholar] [Publisher Link]

[18] Sameer S. Gajghate et al., "Hydrogen-Enriched Direct Injection Diesel Engine Performance, Emission, Combustion, and Sensitivity Analysis Using Ethanol-Nahar Biodiesel Blends," *International Journal of Energy Research*, vol. 2026, no. 1, pp. 1-16, 2026. [CrossRef] [Google Scholar] [Publisher Link]